0.5-bit/s/Hz fine-grained adaptive OFDM modulation for bandlimited underwater VLC

YUNGUI NIE, 1 CHEN CHEN, 2,5 D SVETISLAV SAVOVIĆ, 3 D ZHUO WANG, 4 D RUI MIN, 4 XIAODI YOU, 1 D ZHIHONG ZENG, 2,* D AND GANGXIANG SHEN^{1,6}

Abstract: In this paper, we propose and demonstrate a 0.5-bit/s/Hz fine-grained adaptive orthogonal frequency division multiplexing (OFDM) modulation scheme for bandlimited underwater visible light communication (UVLC) systems. Particularly, integer spectral efficiency is obtained by conventional OFDM with quadrature amplitude modulation (QAM) constellations, while fractional spectral efficiency is obtained by two newly proposed dual-frame OFDM designs. More specifically, OFDM with dual-frame binary phase-shift keying (DF-BPSK) is designed to achieve a spectral efficiency of 0.5 bit/s/Hz, while OFDM with dual-frame dual-mode index modulation (DF-DMIM) is designed to realize the spectral efficiencies of 0.5+n bits/s/Hz with n being a positive integer (i.e., n = 1, 2, ...). The feasibility and superiority of the proposed 0.5-bit/s/Hz fine-grained adaptive OFDM modulation scheme in bandlimited UVLC systems are successfully verified by simulations and proof-of-concept experiments. Experimental results demonstrate that a significant achievable rate gain of 18.6 Mbps can be achieved by the proposed 0.5-bit/s/Hz fine-grained adaptive OFDM modulation in comparison to the traditional 1-bit/s/Hz granularity adaptive OFDM scheme, which corresponds to a rate improvement of 22.1%.

© 2024 Optica Publishing Group under the terms of the Optica Open Access Publishing Agreement

Introduction

Mobile communication has undergone extensive development, and the emergence of each generation of mobile communication technology has aimed to enhance the communication quality, data rate and system capacity. During this period, our daily entertainment has also become increasingly abundant, and the advent of mobile phones has made our lives more convenient, fast and diversified. In recent years, the focus has shifted to the sixth generation (6G) networks, which are committed to using more abundant spectrum resources than the fifth generation (5G) to achieve higher data rate and support for a variety of services such as immersive cloud extended reality and holographic communication [1,2]. As a result, many researchers need to study new and untapped spectrum resources.

In recent years, the increasing demand for underwater activities such as underwater scientific data collection, marine environmental monitoring and unmanned underwater vehicles have made underwater optical wireless communication (OWC) trigger great attention among both academia and industry [3–5]. In addition, as one of the potential key enabling technologies for 6G mobile networks and Internet of Things (IoT) systems, visible light communication (VLC)

https://doi.org/10.1364/OE.513682 Journal © 2024 Received 16 Nov 2023; revised 12 Jan 2024; accepted 13 Jan 2024; published 25 Jan 2024

 $^{^{}I}$ Suzhou Key Laboratory of Advanced Optical Communication Network Technology, School of Electronic and Information Engineering, Soochow University, Suzhou, Jiangsu 215006, China

²School of Microelectronics and Communication Engineering, Chongqing University, Chongqing 400044,

³University of Kragujevac, Faculty of Science, R. Domanovića 12, Kragujevac, Serbia

⁴Center for Cognition and Neuroergonomics, State Key Laboratory of Cognitive Neuroscience and Learning, Beijing Normal University, Zhuhai 519087, China

⁵c.chen@cqu.edu.cn

⁶shengx@suda.edu.cn

^{*}zhihong.zeng@cqu.edu.cn

has attracted great interest from relevant researchers because of its advantages such as abundant and unregulated spectrum resources, low cost, absence of electromagnetic radiation and high physical layer security [6,7]. Underwater VLC (UVLC) is emerging as an attractive alternative to conventional underwater communication technologies such as acoustic communications [8–10]. Moreover, UVLC applying light-emitting diodes (LEDs) has gained more and more attention, primarily due to the rapid development in LED devices that have the functions of lighting and carrying useful information to achieve communication [11–13]. Therefore, UVLC is widely regarded as a promising candidate technology in underwater environments. However, the practical LED-based UVLC system has been limited in achieving a relatively high data rate, mainly due to a large and fundamental challenge faced: limited modulation bandwidth [14]. To overcome the challenge and improve system available data rate for a given modulation bandwidth, high spectral efficiency modulation technologies such as orthogonal frequency division multiplexing (OFDM) with high order constellations can be considered [15–18].

OFDM is a multi-carrier modulation technology renowned for its high spectral efficiency, suitability for adaptive bit loading, resistance to frequency-selective fading, and single-tap equalization, etc., which has been widely used in high-speed UVLC systems [19]. In OFDM, the constellation order assigned to each subcarrier can be the fixed or adaptive. For the fixed OFDM scheme, all subcarriers transmit a fixed number of bits, which cannot adapt to the low-pass frequency response of the bandlimited UVLC systems. For the adaptive OFDM scheme, each subcarrier is adaptively assigned with an appropriate spectral efficiency according to its received signal-to-noise ratio (SNR) [20–23]. However, the granularity of conventional adaptive OFDM schemes using QAM constellations is limited to 1 bit/s/Hz, which might not be sufficient to fully exploit the bandwidth resource of a practical bandlimited UVLC system with a low-pass frequency response [24]. Therefore, a fine-grained adaptive OFDM scheme with fractional spectral efficiency can be designed for efficient bandwidth utilization and capacity improvement of practical bandlimited UVLC system.

Recently, aiming at the shortcomings of OFDM, OFDM with index modulation (OFDM-IM) achieving high energy efficiency has been proposed to obtain better bit error rate (BER) performance than traditional OFDM [25–29]. As a new multi-carrier modulation technology, OFDM-IM mainly divides all subcarriers into multiple subblocks. Within each subblock, a subset of subcarriers are activated to send useful information, while the remaining subcarriers are set to zero. In OFDM-IM, the inactive subcarriers do not require energy consumption, which improves the energy efficiency of the system. However, the existence of some empty subcarriers for OFDM-IM inevitably reduces the spectral efficiency that can be achieved. In order to improve the achievable spectral efficiency, OFDM with dual-mode index modulation (OFDM-DMIM) has been considered in UVLC systems [30,31]. In OFDM-DMIM, all subcarriers are used for transmitting signals. Moreover, the BER performance of UVLC systems applying OFDM-DMIM is largely affected by the choice of two distinguishable constellation sets [32]. In addition, OFDM-DMIM can achieve fractional spectral efficiency and hence has the potential to enhance the achievable rate of the system. However, OFDM-DMIM takes into account the signal transmission of each subcarrier within one frame, which can be affected by the low-pass frequency response of the system and result in different power attenuation for different subcarriers in each subblock

In this paper, for the first time to the best of our knowledge, we propose and investigate a novel 0.5-bit/s/Hz fine-grained adaptive OFDM modulation scheme for bandlimited UVLC systems. By assigning an appropriate spectral efficiency to each subcarrier, the achievable rate of the system can be further improved. To be more specific, integer spectral efficiency can be achieved by traditional OFDM based on quadrature amplitude modulation (QAM) constellations, while fractional spectral efficiency can be obtained by two dual-frame OFDM designs including OFDM with dual-frame binary phase-shift keying (DF-BPSK) achieving 0.5 bit/s/Hz and OFDM with

dual-frame dual-mode index modulation (DF-DMIM) achieving 0.5+n bits/s/Hz ($n=1,2,\cdots$). Both numerical simulations and hardware experiments are conducted to verify the performance of the proposed 0.5 bit/s/Hz fine-grained adaptive OFDM modulation scheme in bandlimited UVLC systems.

2. System model

In this section, we present the schematic diagram of the proposed 0.5-bit/s/Hz fine-grained adaptive OFDM modulation scheme in bandlimited UVLC systems. The schematic diagram of a bandlimited UVLC system using the proposed 0.5-bit/s/Hz fine-grained adaptive OFDM modulation scheme is illustrated in Fig. 1. The proposed 0.5-bit/s/Hz fine-grained adaptive modulation can enhance the achievable rate through assigning a fine-grained spectral efficiency to each subcarrier. Specifically, fine-grained adaptive modulation is performed in the adaptive transmitter (Tx) according to the estimated SNR profile. Channel and SNR estimation is executed in the adaptive receiver (Rx), and the obtained SNR profile is then fed back to the adaptive Tx. Using the feedback SNR profile, the fine-grained adaptive modulation technique for OFDM UVLC systems can be implemented.

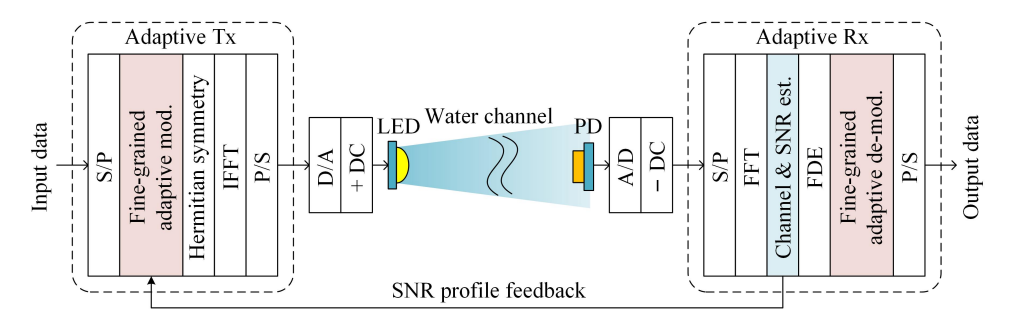


Fig. 1. Schematic diagram of a bandlimited UVLC system using the proposed fine-grained adaptive OFDM modulation scheme. mod.: modulation; est.: estimation; de-mod.: de-modulation.

In the adaptive Tx, the parallel input data are first generated via serial-to-parallel (S/P) conversion. Then, fine-grained adaptive modulation is carried out according to the SNR profile feedback from the adaptive Rx. Specifically, the fine granularity mainly includes integer and fractional spectral efficiencies. For integer spectral efficiency, it is realized by traditional OFDM using QAM constellations. For fractional spectral efficiency, information is carried on two adjacent OFDM frames. The detailed implementation process of fractional spectral efficiency will be discussed later. The 0.5-bit/s/Hz fine-grained adaptive OFDM modulation is implemented by dynamically assigning a fine-grained spectral efficiency to each subcarrier based on the feedback SNR information. Subsequently, a real-valued serial output signal is generated through executing inverse fast Fourier transform (IFFT) with the Hermitian symmetry (HS) and parallel-to-serial (P/S) conversion. After that, the serial digital signal is converted into an analog signal through digital-to-analog (D/A) conversion. In order to ensure the non-negativity of the analog signal, a direct current (DC) bias is further added. Finally, the analog, real-valued and non-negative signal is used to drive an LED transmitter, and the light emitted by the LED propagates through the water channel.

After passing through the water channel, a photo-detector (PD) is adopted to detect the optical signal in the adaptive Rx. The digital electrical signal is obtained by analog-to-digital (A/D) conversion, and the DC bias is removed. Subsequently, S/P conversion is carried out and fast Fourier transform (FFT) is further performed. Then, the SNR profile is generated through SNR estimation, and the obtained SNR profile is fed back to the adaptive Tx to realize the fine-grained

adaptive modulation. After performing frequency-domain equalization (FDE), output data are generated via fine-grained adaptive de-modulation and P/S conversion.

3. 0.5-bit/s/Hz fine-grained adaptive OFDM modulation

In this section, we introduce the principle of the proposed 0.5-bit/s/Hz fine-grained adaptive OFDM modulation scheme. Letting η denote the achievable spectral efficiency, the following two cases are discussed in detail, i.e., $\eta = 0.5$ bit/s/Hz and $\eta = 0.5+n$ bit/s/Hz with $n = 1,2,\ldots$. Specifically, OFDM with DF-BPSK is designed to achieve the spectral efficiency of 0.5 bit/s/Hz, while OFDM with DF-DMIM is proposed to realize the spectral efficiencies of 0.5 + n bits/s/Hz with $n = 1, 2, \ldots$

The reason to consider time-domain dual-frame modulation instead of frequency-domain dual-subcarrier modulation is described as follows. For the frequency-domain dual-subcarrier modulation, the two subcarriers to perform dual-subcarrier BPSK and dual-subcarrier DMIM will inevitably suffer from the adverse effect of the low-pass frequency response of the system, resulting in a degraded BER performance. In contrast, for the time-domain dual-frame modulation, the two consecutive frames with respect to the same subcarrier are used to perform DF-BPSK and DF-DMIM. Since the low-pass frequency response of the system can be considered to be static during a short time period, time-domain dual-frame modulation is not affected by the low-pass frequency response of the system, which can achieve better BER performance than frequency-domain dual-subcarrier modulation.

3.1. Case I: $\eta = 0.5 \text{ bit/s/Hz}$

To achieve the spectral efficiency of 0.5 bit/s/Hz, OFDM with DF-BPSK is designed. Figure 2 shows the frame design of OFDM with DF-BPSK, where *N* denotes the number of data subcarriers in each OFDM frame. As we can see, each subcarrier is only activated once for BPSK symbol transmission in two consecutive frames, and the total number of activated subcarriers for BPSK symbol transmission in each frame is *N*/2.

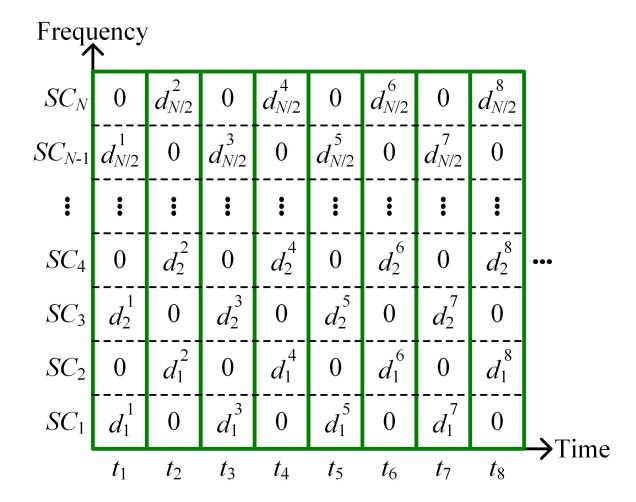


Fig. 2. Frame design of OFDM with DF-BPSK to achieve a spectral efficiency of $\eta = 0.5$ bit/s/Hz.

3.2. Case II: $\eta = 0.5 + n$ bits/s/Hz (n = 1, 2, ...)

To realize the spectral efficiencies of 0.5 + n bits/s/Hz with n = 1, 2, ..., OFDM with DF-DMIM is further proposed, where DMIM is performed with respect to each subcarrier among two adjacent frames.

Figures 3(a) and 3(b) show the principles of OFDM with DF-DMIM modulation and demodulation, respectively. In the OFDM with DF-DMIM modulation process, as shown in Fig. 3(a), the input data are first converted to parallel data via S/P conversion, and then DF-DMIM modulation is performed. To be more specific, the considered DMIM is carried out among two adjacent frames, where one frame is selected to be modulated by the M_A -QAM constellation and the remaining frame is modulated by the M_B -QAM constellation, where M_A and M_B are the constellation orders of constellation A and constellation B, respectively. Moreover, the constellation sets of the constellation mappers A and B are respectively represented by

$$\mathcal{M}_{A} = [d_{1}^{A}, d_{2}^{A}, \dots, d_{M_{A}}^{A}],$$
 (1)

$$\mathcal{M}_{\rm B} = [d_1^{\rm B}, d_2^{\rm B}, \dots, d_{M_{\rm P}}^{\rm B}],$$
 (2)

where d_i^A and d_j^B with $i=1, 2, ..., M_A$ and $j=1, 2, ..., M_B$ denote M_A -QAM constellation symbols and M_B -QAM constellation symbols, respectively. The mapping table of OFDM with DF-DMIM for two adjacent frames is given in Table 1. As we can see, taking the index bit "1" as an example, the second frame is used for modulating M_A -QAM constellation symbols, while the first frame is used for modulating M_B -QAM constellation symbols, and hence the resultant DF-DMIM vector is given by $[d_i^B, d_i^A]$.

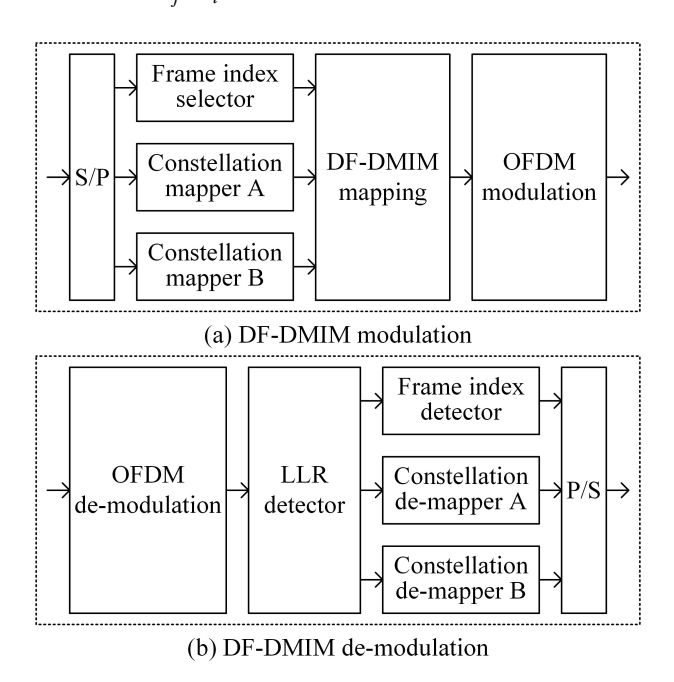


Fig. 3. Principle of OFDM with DF-DMIM: (a) DF-DMIM modulation and (b) DF-DMIM de-modulation.

In the OFDM with DF-DMIM demodulation process, as shown in Fig. 3(b), OFDM demodulation is first carried out and then log-likelihood ratio (LLR) detection is performed for signal detection. Letting y_{κ} (κ =1, 2) express the received signal in the κ -th frame, the LLR value

Table 1. Mapping table of OFDM with DF-DMIM for two adjacent frames

Index bit	Frame index for \mathcal{M}_A	Frame index for \mathcal{M}_B	DF-DMIM vector
0	1	2	$[d_i^{\mathrm{A}}, d_j^{\mathrm{B}}]$
1	2	1	$[d_j^{\mathrm{B}},d_i^{\mathrm{A}}]$

is calculated by

$$\lambda_{\text{DF-DMIM}}^{\kappa} = \ln \left(\sum_{i=1}^{M_{\text{A}}} \exp \left(-\frac{1}{N_0} \left| y_{\kappa} - d_i^{\text{A}} \right|^2 \right) \right)$$
$$- \ln \left(\sum_{j=1}^{M_{\text{B}}} \exp \left(-\frac{1}{N_0} \left| y_{\kappa} - d_j^{\text{B}} \right|^2 \right) \right), \tag{3}$$

where N_0 denotes the noise power. After LLR detection, the index information, the constellation symbols corresponding to M_A -QAM and the constellation symbols corresponding to M_B -QAM are obtained. Subsequently, index bits and the corresponding constellation bits can be generated through the frame index detector, constellation de-mapper A and constellation de-mapper B.

Hence, for bandlimited UVLC systems using DF-DMIM with M_A -QAM and M_B -QAM constellations, the number of index bits can be calculated by $p_I = \lfloor \log_2(C(2,1)) \rfloor = 1$, where $\lfloor \cdot \rfloor$ represents the floor operator and $C(\cdot, \cdot)$ denotes the binomial coefficient. Moreover, the numbers of constellation bits used for modulating M_A -QAM constellation symbols and M_B -QAM constellation symbols are respectively given as follows:

$$p_{\mathcal{A}} = \log_2(M_{\mathcal{A}}),\tag{4}$$

$$p_{\rm B} = \log_2(M_{\rm B}). \tag{5}$$

Therefore, the average achievable spectral efficiency of OFDM with DF-DMIM among two consecutive frames employing M_A -QAM and M_B -QAM constellations is expressed by

$$SE_{\text{DF-DMIM}} = \frac{\left[\log_2(C(2,1))\right] + \log_2(M_A) + \log_2(M_B)}{2}.$$
 (6)

Assuming $M_A = M_B$, (6) can be rewritten by

$$SE_{\text{DF-DMIM}} = \frac{1}{2} + \log_2(\frac{M}{2}),\tag{7}$$

with $M = M_A + M_B$ being the order of the QAM constellation (M-QAM), which is partitioned into two distinguishable sub-constellations, i.e., M_A -QAM and M_B -QAM.

Additionally, the achievable rate of bandlimited UVLC systems applying the proposed 0.5-bit/s/Hz fine-grained adaptive OFDM modulation scheme with the signal bandwidth of BW is obtained by

$$R_{\text{adaptive}} = BW \frac{\sum_{n=1}^{N} BL_{\text{SC},n}}{N},$$
(8)

where $BL_{SC,n}$ indicates the number of the bits that can be transmitted by the n-th subcarrier with n = 1, ..., N. Moreover, the BW of the 0.5-bit/s/Hz fine-grained adaptive OFDM signal for bandlimited UVLC systems can be calculated by

$$BW = S_{\text{AWG}} * \frac{N}{N_{\text{IEFT}}},\tag{9}$$

where S_{AWG} represents the arbitrary waveform generator (AWG) sampling rate in a point-to-point UVLC system, and N_{IFFT} denotes the length of IFFT.

Moreover, the performance of UVLC systems applying OFDM with DF-DMIM is largely depended on the choice of two distinguishable constellations. According the previous works [34,35], interleaving-based constellation partitioning can obtain a relatively larger minimum Euclidean distance between two adjacent constellation points of each sub-constellation which can obtain a better BER performance compared with block-based constellation partitioning. Therefore, interleaving-based constellation partitioning is adopted to obtain the two distinguishable constellations for OFDM with DF-DMIM. To introduce the adopted interleaving-based constellation design for OFDM with DF-DMIM, we consider nine conventional constellations including 4-QAM, 8-QAM, 16-QAM, 32-QAM, 64-QAM, 128-QAM, 256-QAM, 512-QAM, 1024-QAM with the spectral efficiencies of 1.5, 2.5, 3.5, 4.5, 5.5, 6.5, 7.5, 8.5 and 9.5 bits/s/Hz, respectively. Figures 4(a)–4(i) show the dual-mode constellation designs for 4-QAM, 8-QAM, 16-QAM, 32-QAM, 64-QAM, 128-QAM, 512-QAM and 1024-QAM, respectively. It can be clearly seen from Fig. 4 that the *M*-ary constellation is divided into two *M*/2-ary sub-constellations in an interleaved manner.

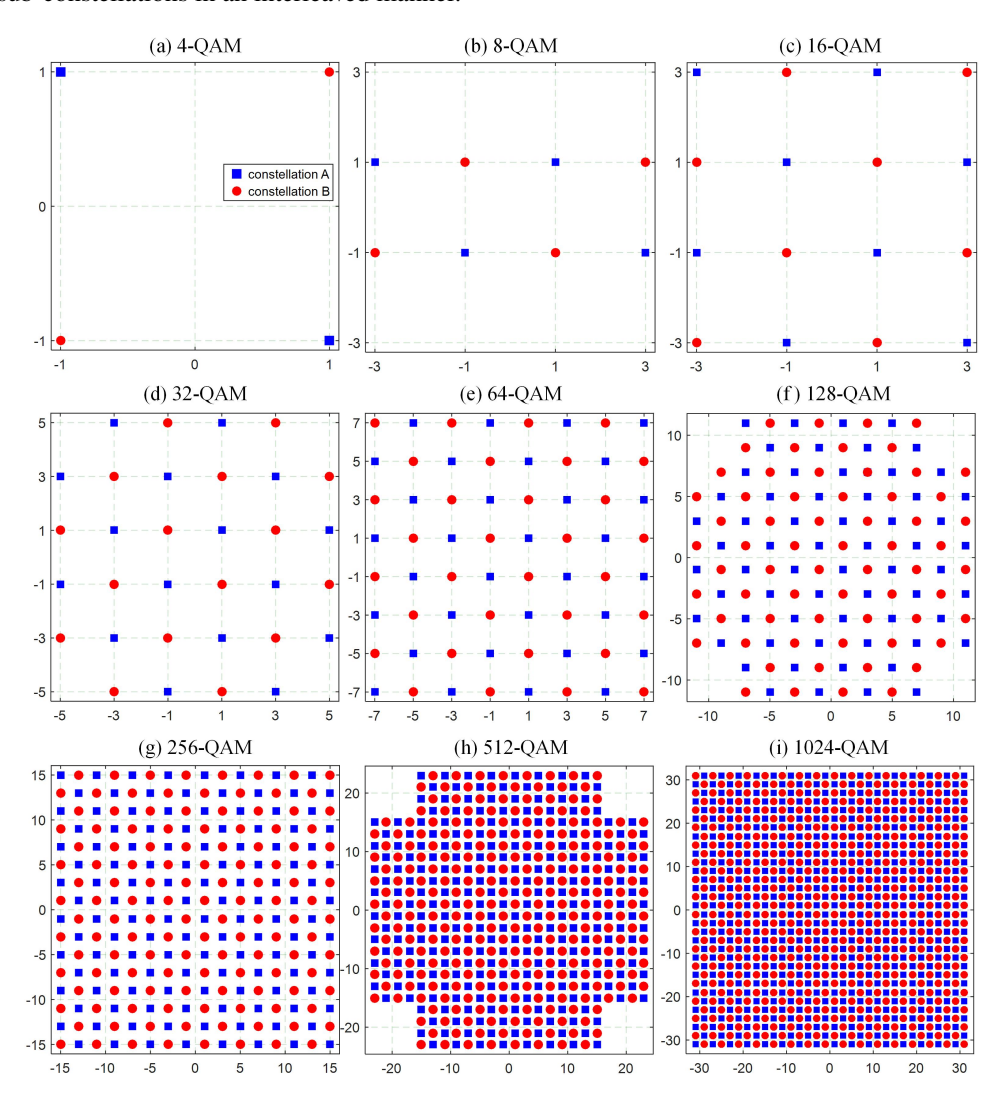


Fig. 4. Dual-mode constellation design for (a) 4-QAM, (b) 8-QAM, (c) 16-QAM, (d) 32-QAM, (e) 64-QAM, (f) 128-QAM, (g) 256-QAM, (h) 512-QAM, and (i) 1024-QAM.

Optics Expires.

4. Simulation results

In this section, we evaluate and compare the performance of the proposed 0.5-bit/s/Hz fine-grained adaptive OFDM modulation over the additive white Gaussian noise (AWGN) channel through numerical simulations. In the simulations, we set the number of IFFT *N*_{IFFT} and data subcarriers *N* to 1024 and 511, respectively. To be more specific, we adopt 4-QAM, 8-QAM, 16-QAM, 32-QAM, 64-QAM, 128-QAM, 512-QAM and 1024-QAM for the proposed OFDM with DF-DMIM scheme, and the corresponding obtained spectral efficiencies are 1.5, 2.5, 3.5, 4.5, 5.5, 6.5, 7.5, 8.5 and 9.5 bits/s/Hz, respectively. Moreover, traditional OFDM based on 2-QAM, 4-QAM, 8-QAM, 16-QAM, 32-QAM, 64-QAM, 128-QAM, 256-QAM, 512-QAM, 1024-QAM can realize the spectral efficiencies of 1, 2, 3, 4, 5, 6, 7, 8, 9 and 10 bits/s/Hz, respectively. In addition, the spectral efficiency of 0.5 bit/s/Hz is achieved by OFDM with DF-BPSK through transmitting signal alternately between two adjacent frames.

We first investigate the BER performance of the proposed 0.5-bit/s/Hz fine-grained adaptive OFDM modulation scheme under different spectral efficiencies over the AWGN channel. Figure 5 shows the BER versus SNR for the 0.5-bit/s/Hz fine-grained adaptive OFDM modulation scheme achieving the spectral efficiencies ranging from 0.5 to 10 bits/s/Hz with a step of 0.5 bit/s/Hz through the AWGN channel. As shown in Fig. 5, the spectral efficiencies of 1, 2, 3, 4, 5, 6, 7, 8, 9 and 10 bits/s/Hz can be realized by conventional OFDM with 2-QAM, 4-QAM, 8-QAM, 16-QAM, 32-QAM, 64-QAM, 128-QAM, 256-QAM, 512-QAM, 1024-QAM, respectively. To be more specific, to reach the 7% forward error correction (FEC) coding limit of BER = 3.8×10^{-3} , the required SNRs for the spectral efficiencies of 1, 2, 3, 4, 5, 6, 7, 8, 9 and 10 bits/s/Hz are 5.5, 8.5, 13.1, 15.2, 18.2, 21.1, 23.9, 26.9, 29.7 and 32.7 dB, respectively. It indicates that the SNR gaps of 3, 4.6, 2.1, 3, 2.9, 2.8, 3, 2.8 and 3 dB are achieved with the increase of the spectral efficiencies from 1 to 10 bits/s/Hz with a step of 1 bit/s/Hz. Furthermore, the required SNR of 0.5 bit/s/Hz based on OFDM with DF-BPSK to reach the target BER = 3.8×10^{-3} is 2.5 dB. Additionally, the required SNRs achieved by OFDM with DF-DMIM achieving the spectral efficiencies of 1.5 to 9.5 bits/s/Hz with a step of 1 bit/s/Hz are 6.6, 11.5, 14.1, 17.2, 20.5, 23.5, 26.6, 29.5 and 32.7 dB, respectively. Moreover, the required SNR thresholds to reach target BER of 3.8×10^{-3} for the proposed 0.5-bit/s/Hz fine-grained adaptive OFDM modulation scheme achieving the spectral efficiencies of 0.5 to 10 bits/s/Hz with a step of 0.5 bit/s/Hz are summarized in Table 2.

Table 2. SNR threshold for different spectral efficiencies to reach BER

$= 3.8 \times 10^{-3}$							
η (bit/s/Hz)	0.5	1	1.5	2	2.5	3	3.5
λ (dB)	2.5	5.5	6.6	8.5	11.5	13.1	14.1
η (bit/s/Hz)	4	4.5	5	5.5	6	6.5	7
λ (dB)	15.2	17.2	18.2	20.5	21.1	23.5	23.9
η (bit/s/Hz)	7.5	8	8.5	9	9.5	10	
λ (dB)	26.6	26.9	29.5	29.7	32.7	32.7	

According to the above BER performance analysis, we further investigate and compare the SNR gap of adjacent spectral efficiencies under different spectral efficiencies. Figure 6 shows the SNR gap of adjacent spectral efficiencies versus spectral efficiency for the 0.5-bit/s/Hz fine-grained adaptive OFDM modulation scheme over the AWGN channel. Moreover, η ranges from 0.5 to 9.5 bits/s/Hz with a step of 1 bit/s/Hz. The obtained SNR threshold can be represented as $\lambda_{th}(\eta)$, and hence $\lambda_{th}(\eta+0.5)-\lambda_{th}(\eta)$ denotes SNR gap of two adjacent spectral efficiencies. As shown in Fig. 6, it can be clearly observed that the values of $\lambda_{th}(\eta+0.5)-\lambda_{th}(\eta)$ are gradually decreased

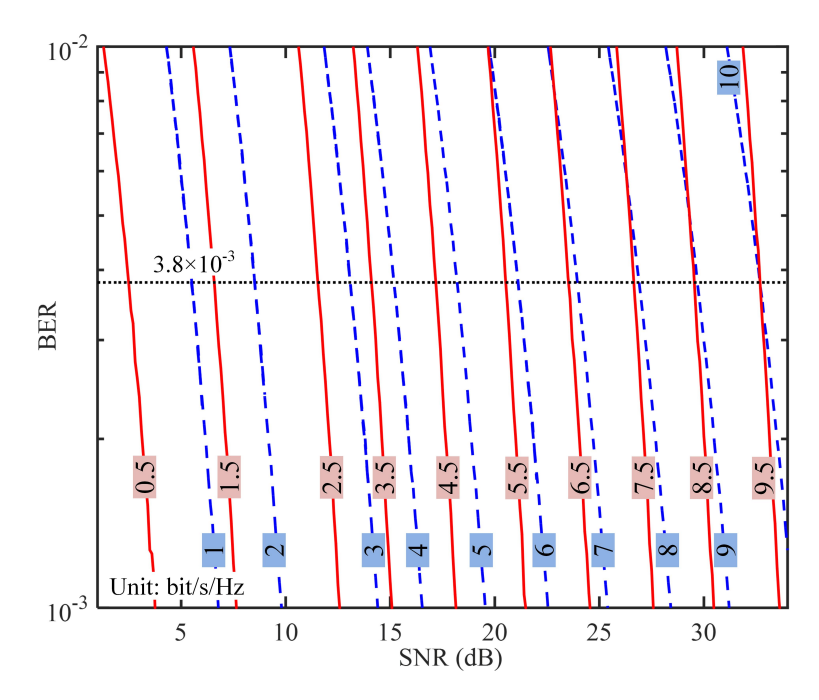


Fig. 5. Simulation BER vs. SNR for the proposed 0.5-bit/s/Hz fine-grained adaptive OFDM modulation scheme over the AWGN channel, where the spectral efficiency is ranging from 0.5 to 10 bits/s/Hz with a granularity of 0.5 bit/s/Hz.

with the increase of spectral efficiency. To be more specific, when the spectral efficiency of 2.5 bits/s/Hz is considered, the corresponding value of $\lambda_{th}(\eta + 0.5) - \lambda_{th}(\eta)$ is 1.6.

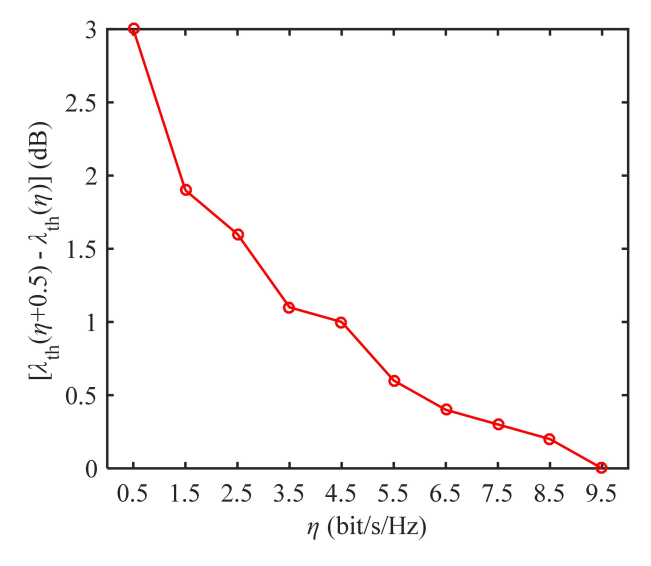


Fig. 6. SNR gap in dB of adjacent spectral efficiencies vs. spectral efficiency over the AWGN channel.

5. Experimental results

In this section, we investigate and compare the performance of the proposed 0.5-bit/s/Hz fine-grained adaptive OFDM modulation scheme in bandlimited UVLC systems via hardware experiments. For comparison, traditional adaptive OFDM modulation scheme with 1-bit/s/Hz granularity is considered in the performance evaluation. Moreover, considering the additional complexity and insignificant rate improvement of power loading over the intensity modulation/direct detection (IM/DD) channel [36], only bit loading is considered in the following experimental demonstration.

Fig. 7 depicts the experimental setup of a point-to-point UVLC system using a blue mini-LED and the inset shows the photo of the overall experimental system. As we can see, firstly, the transmitted signal is generated offline via MATLAB. The obtained transmitted signal is then loaded into an AWG (Tektronix AFG31102) with a sampling rate of 500 MSa/s. Subsequently, a DC bias current of 120 mA is combined with the AWG output signal through a bias-tee (bias-T, Mini-Circuits ZFBT-6GW+). The combined signal is used for driving the blue mini-LED (HCCLS2021CHI03). The light from the blue mini-LED passes through a biconvex lens with a diameter of 12.7 mm and a focal length of 20 mm, and then propagates through the 1-m water tank. The overall transmission distance is 135 cm. At the receiving end, the optical signal is directly detected by a photodetector (PD, Thorlabs PDA10A2), where the bandwidth and the active area of PD are 150 MHz and 0.8 mm², respectively. Moreover, to align the blue mini-LED and the PD, another biconvex lens is also adopted to obtain a relatively high SNR. Subsequently, a digital storage oscilloscope (DSO, LeCroy WaveSurfer432) with a sampling rate of 2.5 GSa/s is employed to record the received electrical signal. Finally, the recorded signal is demodulated offline via MATLAB. In OFDM modulation, the size of IFFT is set to 256 and the signal bandwidth is adjusted by changing the number of subcarriers for data transmission.

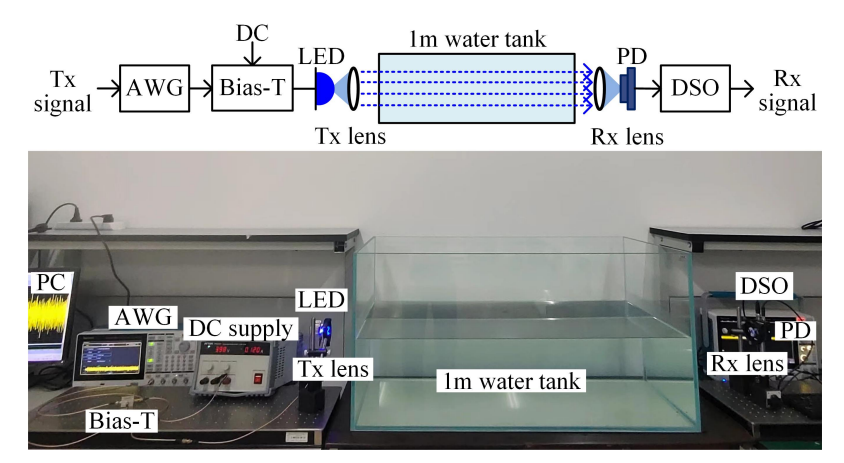


Fig. 7. Experimental setup of a point-to-point UVLC system using a blue mini-LED. AWG: arbitrary waveform generator, DSO: digital storage oscilloscope.

Fig. 8 shows the measured frequency response of the experimental UVLC system. It can be clearly seen that the experimental system exhibits a notable low-pass frequency response, and the corresponding -3 dB bandwidth is about 35 MHz. The key experimental parameters are given in Table 3.

Fig. 9 depicts the received SNR under six different signal bandwidths of 31, 41, 51, 61, 70 and 80 MHz at the peak-to-peak voltage (Vpp) of 1 V. As we can see, the overall SNR is gradually reduced with the increase of signal bandwidth and the high-frequency subcarriers generally have a relatively low SNR.

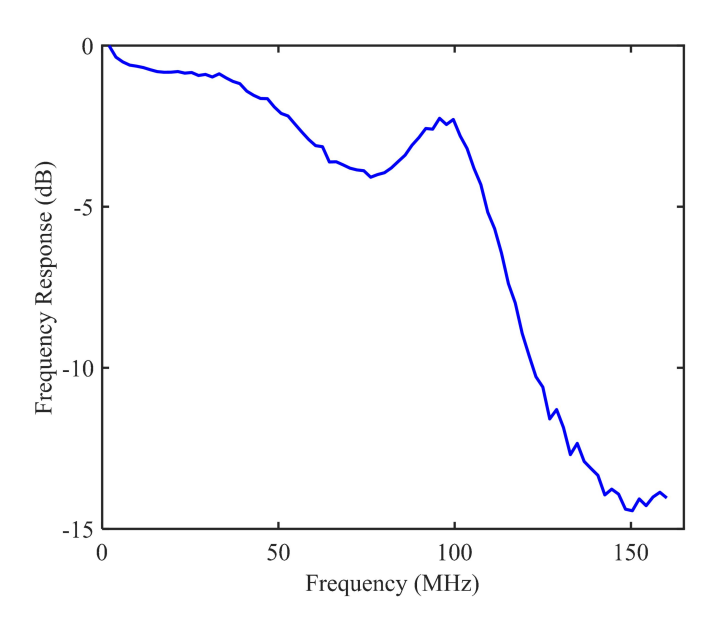


Fig. 8. Measured frequency response of the experimental UVLC system.

Table	3.	Experimental	parameters

Parameter	Value
The number of IFFT/FFT	256
The transmission distance	135 cm
AWG sampling rate	500 MSa/s
DC bias current	120 mA
Diameter of biconvex lenses	12.7 mm
Focal length of biconvex lenses	20 mm
Bandwidth of PD	150 MHz
Active area of PD	0.8 mm^2
DSO sampling rate	2.5 GSa/s

Fig. 10 shows the bit loading for the signal bandwidth of 61 MHz at Vpp = 1 V. It can be found that the traditional 1-bit/s/Hz granularity adaptive OFDM modulation scheme can only load integer bits to each subcarrier, while the proposed 0.5-bit/s/Hz fine-grained adaptive OFDM modulation scheme can load both integer and fractional bits to each subcarrier. Specifically, for the low-frequency subcarriers, only 2 bits can be loaded when using the traditional 1-bit/s/Hz granularity adaptive OFDM modulation scheme, while 2.5 bits can be loaded when applying the proposed 0.5-bit/s/Hz fine-grained adaptive OFDM modulation scheme. The corresponding constellation diagrams of different loaded bits are given in the inset in Fig. 10. Moreover, it can be inferred that more bits might be further loaded with a finer granularity such as 0.25-bit/s/Hz by using higher modes OFDM-IM [32]. Nevertheless, the use of a finer granularity might not be able to further bring a significant rate improvement compared with that using a granularity of 0.5 bit/s/Hz.

Fig. 11 shows the achievable rate versus signal bandwidth for different Vpp values. It can be found that, for both traditional 1-bit/s/Hz granularity adaptive OFDM and the proposed 0.5-bit/s/Hz fine-grained adaptive OFDM, the achievable rates are first increased and then decreased

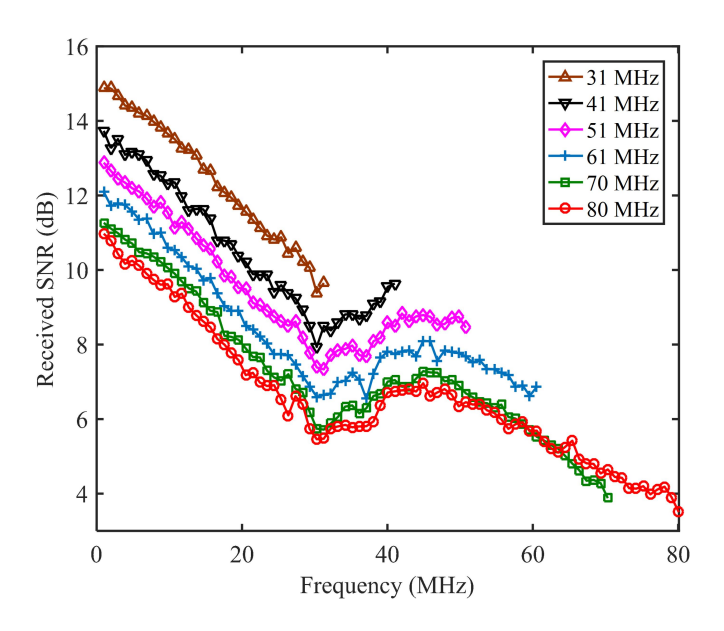


Fig. 9. Received SNR for different signal bandwidths at Vpp = 1 V.

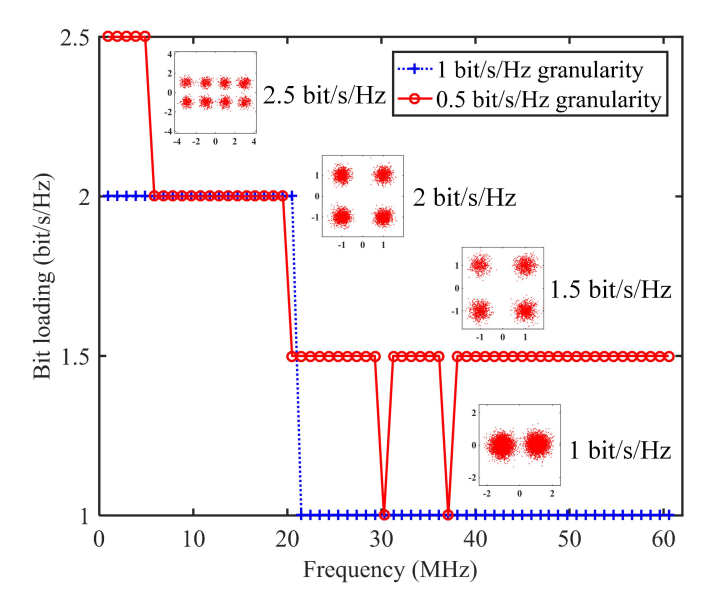


Fig. 10. Bit loading for the signal bandwidth of 61 MHz at Vpp = 1 V.

with the increase of the signal bandwidths, indicating the existence of an optimal signal bandwidth to achieve the maximum rate for each scheme. Moreover, the achievable rates of 0.5-bit/s/Hz fine-grained adaptive OFDM are always higher than the 1-bit/s/Hz granularity adaptive OFDM modulation. To be more specific, for the case of Vpp = 1 V, as shown in Fig. 11(a), a maximum achievable rate of 84.0 Mbps is obtained with the signal bandwidth of 51 MHz for 1-bit/s/Hz granularity adaptive OFDM modulation, while a maximum achievable rate of 102.1 Mbps is achieved for 0.5-bit/s/Hz fine-grained adaptive OFDM modulation with the signal bandwidth of 61 MHz. For the case of Vpp of 1.5 and 2 V, the maximum achievable rates are respectively increased from 152.3 to 169.3 and 324.4 to 347.7 Mbps, when applying 0.5-bit/s/Hz fine-grained adaptive OFDM in comparison to traditional 1-bit/s/Hz granularity adaptive OFDM. Similarly, the maximum achievable rates are respectively increased from 370.1 to 394.5 and 433.6 to 457.0 Mbps at the Vpp of 2.5 and 3 V, when 0.5-bit/s/Hz fine-grained adaptive OFDM is considered. According to Figs. 11(a)-11(e), we can conclude that there is an optimal signal bandwidth to achieve the maximum achievable rates for 1-bit/s/Hz granularity adaptive OFDM modulation and 0.5-bit/s/Hz fine-grained adaptive OFDM modulation in bandlimited UVLC systems. Moreover, the maximum achievable rate of 0.5-bit/s/Hz fine-grained adaptive OFDM modulation can be achieved under the same or higher signal bandwidth in comparison to 1-bit/s/Hz granularity adaptive OFDM modulation.

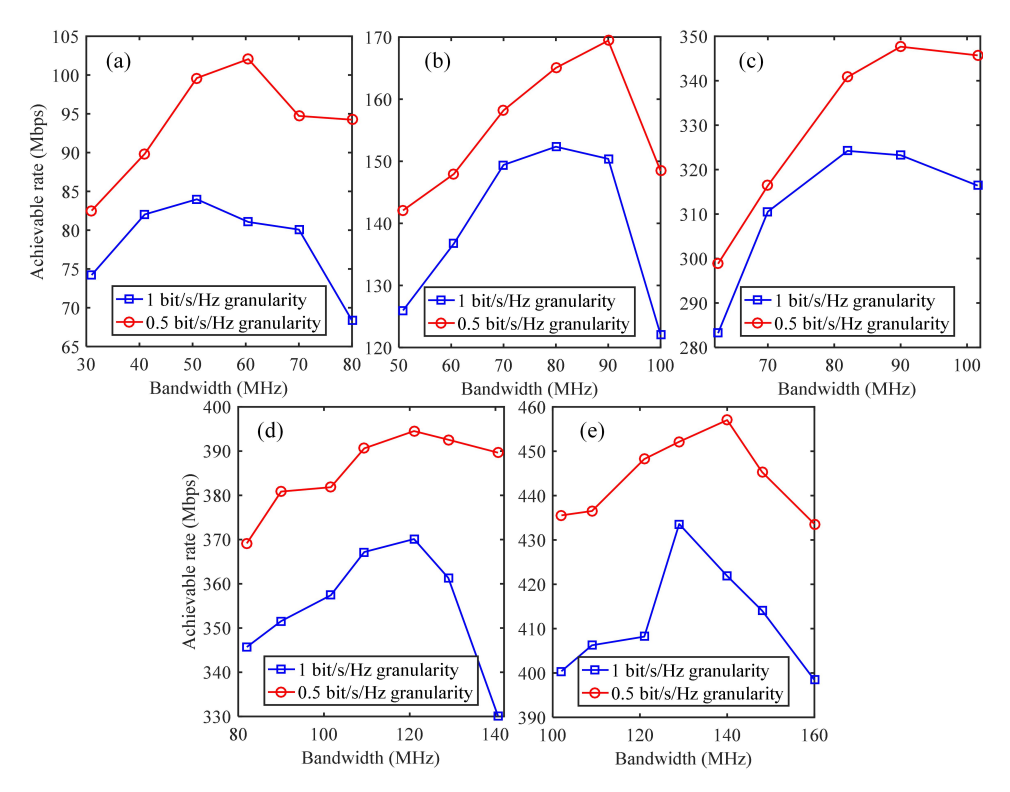


Fig. 11. Achievable rate vs. signal bandwidth for (a) Vpp = 1 V, (b) Vpp = 1.5 V, (c) Vpp = 2 V, (d) Vpp = 2.5 V, and (e) Vpp = 3 V.

Fig. 12 shows the rate gain and the rate gain percentage versus Vpp for 0.5-bit/s/Hz fine-grained adaptive OFDM in comparison to traditional 1-bit/s/Hz granularity adaptive OFDM. As we can see, the rate gain is generally within the range of about 15 to 25 Mbps, while the rate gain percentage is gradually reduced with the increase of Vpp. To be more specific, the rate gain of 18.6 Mbps at the Vpp of 1 V is achieved, which is corresponding to a 22.1% rate improvement.

For the case of Vpp = 1.5 and 2 V, the rate gains of 15.6 and 23.4 Mbps are achieved, which are corresponding to 10.3% and 7.7% improvements of the achievable rate, respectively. Similarly, in comparison to 1-bit/s/Hz granularity adaptive OFDM scheme, the rate improvements of 7.5% and 5.4% realized by 0.5-bit/s/Hz fine-grained adaptive OFDM are respectively obtained, when the rate gains are 24.4 and 23.4 Mbps at the Vpp of 2.5 and 3 V. With the increase of Vpp from 1 to 3 V, the achievable rate is gradually increased while the rate gain remains relatively stable, and hence the rate gain percentage is inevitably reduced with the increase of Vpp, i.e., the increase of SNR. It can be clearly observed from Fig. 12 that the 0.5-bit/s/Hz fine-grained adaptive OFDM scheme is more advantageous in the relatively small SNR region.

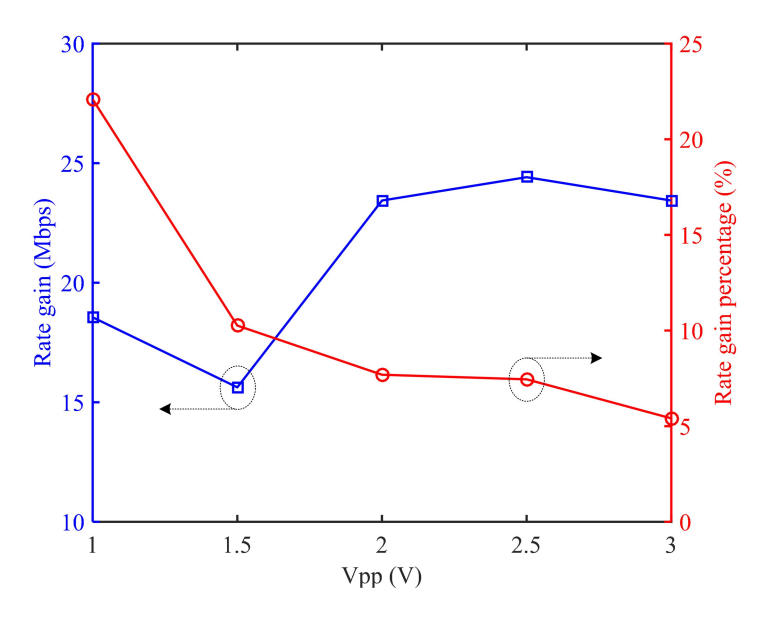


Fig. 12. Rate gain and rate gain percentage vs. Vpp for 0.5-bit/s/Hz fine-grained adaptive OFDM in comparison to traditional 1-bit/s/Hz granularity adaptive OFDM.

6. Conclusion

In this paper, we have proposed and evaluated a 0.5-bit/s/Hz fine-grained adaptive OFDM modulation scheme for bandlimited UVLC systems, where integer and fractional spectral efficiencies are considered to enhance the achievable rate of the system. Specifically, integer spectral efficiencies can be achieved by traditional OFDM based on QAM constellations, while fractional spectral efficiencies including 0.5 bit/s/Hz and 0.5+n bits/s/Hz can be achieved by OFDM with DF-BPSK and OFDM with DF-DMIM, respectively. The obtained simulation and experimental results verify the superiority of the proposed 0.5-bit/s/Hz fine-grained adaptive OFDM modulation scheme for bandlimited UVLC systems in comparison to the traditional 1-bit/s/Hz granularity adaptive OFDM modulation scheme. Therefore, the proposed 0.5-bit/s/Hz fine-grained adaptive OFDM modulation scheme can be a promising candidate for practical bandlimited UVLC systems.

Funding. National Natural Science Foundation of China (61901065, 62271091); Natural Science Foundation of Chongqing (cstc2021jcyj-msxmX0480).

Disclosures. The authors declare that there are no conflicts of interest related to this article.

Data availability. Data underlying the results presented in this paper are not publicly available at this time but may be obtained from the authors upon reasonable request.

References

- N. Chi, Y. Zhou, Y. Wei, et al., "Visible light communication in 6G: Advances, challenges, and prospects," IEEE Veh. Technol. Mag. 15(4), 93–102 (2020).
- W. Wen, X. Peng, C. Chen, et al., "Joint optimization of bitrate selection and beamforming for holographic video cooperative streaming in VLC systems," IEEE Commun. Lett. 27(10), 2608–2612 (2023).
- Z. Zeng, S. Fu, H. Zhang, et al., "A survey of underwater optical wireless communications," IEEE Commun. Surv. Tuts. 19(1), 204–238 (2017).
- 4. W. Liu, L. Zhang, N. Huang, *et al.*, "Wide dynamic range signal detection for underwater optical wireless communication using a PMT detector," Opt. Express **31**(15), 25267–25279 (2023).
- B. Deng, J. Wang, Z. Wang, et al., "Polarization multiplexing based UOWC systems under bubble turbulence," J. Lightwave Technol. 41(17), 5588–5598 (2023).
- T. Komine and M. Nakagawa, "Fundamental analysis for visible-light communication system using LED lights," IEEE Trans. Consum. Electron. 50(1), 100–107 (2004).
- S. Rajagopal, R. D. Roberts, and S.-K. Lim, "IEEE 802.15.7 visible light communication: Modulation schemes and dimming support," IEEE Commun. Mag. 50(3), 72–82 (2012).
- M. F. Ali, D. N. K. Jayakody, and Y. Li, "Recent trends in underwater visible light communication (UVLC) systems," IEEE Access 10, 22169–22225 (2022).
- Y. Qian, C. Chen, P. Du, et al., "Hybrid space division multiple access and quasi-orthogonal multiple access for multi-user underwater visible light communication," IEEE Photonics J. 15(4), 1–7 (2023).
- J. Wang, C. Chen, B. Deng, et al., "Dual-mode spatial division multiplexing with geometric constellation shaping for UVLC," in Asia Communications and Photonics Conference/International Photonics and Optoelectronics Meetings (2023), pp. 1–4.
- A. Kumar, S. Al-Kuwari, D. N. K. Jayakody, et al., "Security performance analysis of a NOMA-assisted underwater VLC system under imprecise channel estimations," IEEE Access 10, 117021–117032 (2022).
- 12. S. Hessien, S. C. Tokgoz, N. Anous, *et al.*, "Experimental evaluation of OFDM-based underwater visible light communication system," IEEE Photonics J. **10**(5), 1–13 (2018).
- 13. M. Elamassie, F. Miramirkhani, and M. Uysal, "Performance characterization of underwater visible light communication," IEEE Trans. Commun. 67(1), 543–552 (2019).
- J. Wang, C. Chen, B. Deng, et al., "Enhancing underwater VLC with spatial division transmission and pairwise coding," Opt. Express 31(10), 16812–16832 (2023).
- 15. R. Mesleh, H. Elgala, and H. Haas, "On the performance of different OFDM based optical wireless communication systems," J. Opt. Commun. Netw. 3(8), 620–628 (2011).
- M. Z. Afgani, H. Haas, H. Elgala, et al., "Visible light communication using OFDM," in Int. Conf. Testbeds Res. Infrastructures Develop. Netw. Communities (2006), 129–134.
- A. A. Purwita, M. D. Soltani, M. Safari, et al., "Terminal orientation in OFDM-based LiFi systems," IEEE Trans. Wireless Commun. 18(8), 4003–4016 (2019).
- J. Chen, B. Deng, C. Chen, et al., "Efficient capacity enhancement using OFDM with interleaved subcarrier number modulation in bandlimited UOWC systems," Opt. Express 31(19), 30723–30734 (2023).
- 19. L. Yang, W. Xu, J. Lai, et al., "OFDM-based underwater visible light communication: system construction and performance analysis," in *Int. Conf. on Optical Commun. and Netw.* (2021), pp. 1–3.
- A. Radosevic, R. Ahmed, T. M. Duman, et al., "Adaptive OFDM modulation for underwater acoustic communications: Design considerations and experimental results," IEEE J. Oceanic Eng. 39(2), 357–370 (2014).
- Y. Hong, T. Wu, and L.-K. Chen, "On the performance of adaptive MIMO-OFDM indoor visible light communications," IEEE Photonics Technol. Lett. 28(8), 907–910 (2016).
- H. Farahneh, F. Hussain, and X. Fernando, "Performance analysis of adaptive OFDM modulation scheme in VLC vehicular communication network in realistic noise environment," J Wireless Com Network 2018(1), 243 (2018).
- C. Chen, Y. Nie, M. Liu, et al., "Digital pre-equalization for OFDM-based VLC systems: Centralized or distributed?" IEEE Photonics Technol. Lett. 33(19), 1081–1084 (2021).
- I. Kim, H. L. Lee, B. Kim, et al., "On the use of linear programming for dynamic subchannel and bit allocation in multiuser OFDM," in Global Telecommunications Conf. (IEEE, 2001), pp. 3648–3652.
- E. Basar and E. Panayirci, "Optical OFDM with index modulation for visible light communications," in *Int. Workshops Opt. Wireless Commun.* (2015), pp. 11–15.
- 26. M. Wen, X. Cheng, M. Ma, et al., "On the achievable rate of OFDM with index modulation," IEEE Trans. Signal Process. 64(8), 1919–1932 (2016).
- E. Basar, U. Aygolu, E. Panayirci, et al., "Orthogonal frequency division multiplexing with index modulation," IEEE Trans. Signal Process. 61(22), 5536–5549 (2013).
- F. Ahmed, Y. Nie, C. Chen, et al., "DFT-spread OFDM with quadrature index modulation for practical VLC systems," Opt. Express 29(21), 33027–33036 (2021).
- C. Chen, X. Deng, Y. Yang, et al., "Experimental demonstration of optical OFDM with subcarrier Index modulation for IM/DD VLC." in Asia Communications and Photonics Conference (2019), paper M4A.40.
- T. Mao, R. Jiang, and R. Bai, "Optical dual-mode index modulation aided OFDM for visible light communications," Opt. Commun. 391, 37–41 (2017).

- 31. Y. Nie, J. Chen, W. Wen, et al., "Orthogonal subblock division multiple access for OFDM-IM-based multi-user VLC systems," Photonics 9(6), 373 (2022).
- 32. X. Zhang, H. Bie, Q. Ye, *et al.*, "Dual-mode index modulation aided OFDM with constellation power allocation and low-complexity detector design," IEEE Access **5**, 23871–23880 (2017).
- 33. Y. Acar and S. A. Colak, "Receiver design for dual-mode index modulation aided OFDM," in *Int. Conf. on Advanced Commun. Technol. and Netw.* (2019), pp. 1–5.
- 34. J. Zhao, C. Qin, M. Zhang, *et al.*, "Investigation on performance of special-shaped 8-quadrature amplitude modulation constellations applied in visible light communication," Photonics Res. 4(6), 249–256 (2016).
- 35. C. Chen, Y. Nie, F. Ahmed, *et al.*, "Constellation design of DFT-S-OFDM with dual-mode index modulation in VLC," Opt. Express **30**(16), 28371–28384 (2022).
- 36. S. Mardanikorani, X. Deng, and J.-P. M. G. Linnartz, "Sub-carrier loading strategies for DCO-OFDM LED communication," IEEE Trans. Commun. 68(2), 1101–1117 (2020).